

# Optimal Trajectory Generation using Model Predictive Control for Aerially Towed Cable Systems

Liang Sun<sup>1</sup>, John D. Hedengren<sup>2</sup>, and Randal W. Beard<sup>3</sup>  
*Brigham Young University, Provo, UT, 84602, USA*

This paper studies trajectory generation for an aircraft that tows an aerial body using a flexible cable. The major contributions of this paper include model validation for a lumped mass extensible cable using flight test data, and optimal trajectory generation for the towed cable system with tension constraints using model predictive control. The optimization problem is formulated using a combination of the squared-error and  $L_1$ -norm objective functions. Different desired circular trajectories of the towed body are used to calculate optimal trajectories for the towing vehicle subject to performance limits and wind disturbances. Trajectory generation for transitions from a straight and level flight into an orbit is also presented. This paper gives a framework for specifying an arbitrary flight path for the towed body by optimizing the action of the towing vehicle subject to constraints and disturbance.

## Nomenclature

$A$	cross-sectional area of the cable, $\text{m}^2$
$\alpha_j$	angle of attack of the $j^{\text{th}}$ cable link, rad
$\mathbf{a}_m$	mothership acceleration in the inertial frame, $\text{m}^2/\text{s}$
$C_{D_{dr}}$	drag coefficient of the drogue

---

<sup>1</sup> PhD Student, Electrical and Computer Engineering, 459 CB, Brigham Young University, Provo, UT 84602, USA.

<sup>2</sup> Assistant Professor, Chemical Engineering, 350R CB, Brigham Young University, Provo, UT 84602, USA.

<sup>3</sup> Professor, Electrical and Computer Engineering, 450 CB, Brigham Young University, Provo, Utah 84602, USA, Senior Member AIAA.

$C_{D_j}$	drag coefficient of the $j^{\text{th}}$ cable link
$C_{L_{dr}}$	lift coefficient of the drogue
$C_{L_j}$	lift coefficient of the $j^{\text{th}}$ cable link
$\mathbf{c}_y, \mathbf{c}_u$	cost weights of $\mathbf{y}$ and $\mathbf{u}$
$\mathbf{d}$	parameters or unmeasured disturbances
$E$	Young's modulus, GPa
$\mathbf{e}_3$	unit vector in Down direction in NED coordinates
$\mathbf{e}_{D_j}$	unit vector defining the direction of the aerodynamic drag of the $j^{\text{th}}$ cable link
$\mathbf{e}_{L_j}$	unit vector defining the direction of the aerodynamic lift of the $j^{\text{th}}$ cable link
$\mathbf{e}_{hi}, \mathbf{e}_{lo}$	slack variables
$\mathbf{e}_{L_{dr}}$	unit vector representing the direction of the aerodynamic lift force on the drogue
$\mathbf{f}$	equations of motion
$\mathbf{F}_{dr}^{aero}$	aerodynamic forces acting on the drogue, N
$\mathbf{F}_j^{aero}$	aerodynamic forces acting on the $j^{\text{th}}$ cable link, N
$g$	gravitational force exerted on a unit mass at Earth sea level, $\text{m}^2/\text{s}$
$\gamma_a$	air mass referenced flight path angle, rad
$\mathbf{G}_{dr}$	gravity of the drogue, N
$\mathbf{g}_{iec}$	inequality constraints
$\mathbf{G}_j$	gravity of the $j^{\text{th}}$ cable link, N
$h_0$	desired constant altitude of the drogue, m
$j$	sequence number of cable links or joints
$L_0$	unstretched length of the cable, m
$\ell_j$	stretched length of the $j^{\text{th}}$ cable link, m
$\mathbf{l}_j$	vector between the $(j - 1)^{\text{th}}$ and $j^{\text{th}}$ joints of the cable, m

$\ell_0$	unstretched length of each cable link, m
$m_{dr}$	mass of the drogue, kg
$m_j$	mass of the $j^{\text{th}}$ cable link, kg
$M_{n_j}$	Mach number normal to the $j^{\text{th}}$ cable link
$M_{p_j}$	Mach number parallel to the $j^{\text{th}}$ cable link
$N$	number of cable links
$\mathbf{p}_{dr}(t)$	actual drogue position at time $t$ in the inertial frame, m
$\mathbf{p}_{dr}^d(t)$	desired drogue position at time $t$ in the inertial frame, m
$\Phi$	objective function value
$\phi$	bank angle, rad
$\mathbf{p}_j$	position of the $j^{\text{th}}$ cable joint in the inertial frame, m
$\mathbf{p}_m$	mothership position in the inertial frame, m
$\psi$	heading angle, rad
$r_{dr}^d$	desired orbit radius of the drogue, m
$\rho$	atmospheric density, kg/m <sup>3</sup>
$S_{dr}$	planform area of the drogue wing, m <sup>2</sup>
$\mathbf{sp}_{hi}, \mathbf{sp}_{lo}$	higher and lower dead-band setpoints
$t_0$	starting time of the simulation, s
$t_1$	ending time of the simulation, s
$t_a$	starting time of the transition, s
$\tau$	response time constant of the desired controlled variables
$\theta$	orbital angle, rad
$\mathbf{T}_j$	cable tension exerted on the $j^{\text{th}}$ joint by the $(j - 1)^{\text{th}}$ joint, N
$T_p^a$	drogue orbital period with constant airspeed, s

$T_p^g$	drogue orbital period with constant ground speed, s
$\mathbf{u}$	inputs
$V_a$	magnitude of mothership airspeed, m/s
$v_{dr}^a$	magnitude of the desired drogue airspeed, m/s
$v_{dr}^g$	magnitude of the desired ground speed of the drogue, m/s
$\mathbf{v}_{dr}^s$	drogue velocity relative to the wind frame, m/s
$\mathbf{v}_j^s$	velocity of the $j^{\text{th}}$ cable link relative to the wind frame, m/s
$\mathbf{v}_m$	mothership velocity relative to the wind frame, m/s
$\mathbf{w}_c$	constant component of the wind in the inertial frame, m/s
$\mathbf{w}_{hi}, \mathbf{w}_{lo}$	weights on the controlled variables outside the dead-bands
$\mathbf{x}$	states of the equations of motion
$\mathbf{y}$	controlled variables
$\mathbf{y}_{hi}, \mathbf{y}_{lo}$	higher and lower dead-bands of the controlled variables

## I. Introduction

Miniature Air Vehicles (MAVs) which are characterized by relatively low cost, superior portability, and in some cases, improved stealth, have the potential to open new application areas and broaden the availability of Unmanned Aircraft System (UAS) technology. MAVs are typically battery powered, hand launched and belly landed, and therefore may not require a runway for take-off or landing. Backpackable MAVs can be used in gathering time-critical, over-the-hill Intelligence, Surveillance and Reconnaissance (ISR) information. However retrieving the MAV may be problematic because landing the vehicle near the operator could disclose his/her location. Another potential application of MAVs is collecting disaster damage information. Again for this application, retrieval of the MAV after it has performed its mission is difficult because target locations are often inaccessible, and the MAV may not have enough fuel to return to its home position. The relatively low cost of MAVs suggests that they may be expendable, thereby removing the need for recovery. However, even if the costs are low, MAVs still contain critical and often classified technology which

needs to be kept out of enemy hands. One option is to destroy the MAV or damage the electronics so that it cannot be reused or reverse engineered. However, most of the solutions that have been proposed require additional payload on the MAV. Cost considerations and the potential that MAV technology could fall into enemy hands will limit the use of this technology.

In this paper, an aerial retrieval strategy for MAVs is proposed to solve the problem. Figure 1 shows the basic concept proposed in this paper, where the towing vehicle (mothership) enters an orbit designed to cause the towed body (drogue) to execute an orbit of smaller radius and lower speed (less than the nominal speed of the MAV). The MAV then enters the drogue orbit at its nominal airspeed and overtakes the drogue with a relatively low closing speed.

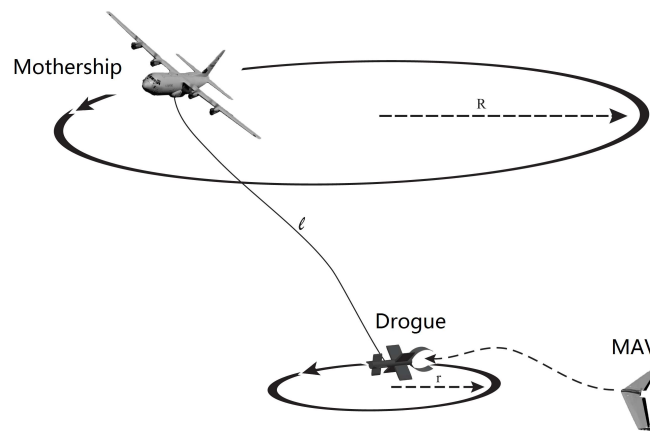


**Fig. 1** This figure shows the baseline concept described in the paper. The mothership recovers a MAV by towing a long cable attached to a drogue. The drogue is actuated and can maneuver and communicate with the MAV to facilitate successful capture. The MAV uses vision-based guidance strategies to intercept the drogue.

The system shown in Fig. 1 is a typical circularly towed cable-body system which has been studied since D. Bernoulli (1700-1782) and L. Euler (1707-1783) who focused on the study of linearized solutions of a whirling string. Modern studies began with Kolodner [1] who made a detailed mathematical study of the free whirling of a heavy chain with the tow-point fixed. In subsequent decades, the studies of the towed cable system focused on the analysis of equilibrium and stability of the system, and dynamic modeling approaches for the cable with which the motion of towing point is a straight line or orbital path [2–5]. In the recent years, Williams et al. made major contributions

to the study of the towed body system. Williams and Trivailo [6, 7] gave a detailed description of the dynamics of circularly towed drogues and designed strategies for moving from one orbit configuration to another. Williams and Ockels [8] employed this approach to the problem of lifting payloads using multiple fixed-wing aircraft. Williams [9] also presented a numerical approach to mitigate the disturbance of a crosswind on the periodic solution of the cable tip using a combination of towing vehicle manipulation and cable length regulation.

An appropriate mathematical model that compromises between complexity and accuracy is the foundation for further studies of the towed cable system like developing control strategies. The central problem in modeling for towed cable systems is the way how the cable is treated. In this paper, as recommended in [10], the finite element approach is used to model the cable, which is treated as a series of  $N < \infty$  rigid links with lumped masses at the joints. Many researchers developed the equations of motion for towed cable systems using Lagrange's method [11, 12] and Kane's equations [13, 14], which do not scale well for a large number of links. Newton's second law is a fundamental and widely used tool to formulate equations of motion for dynamical systems. However, this method was seldom used to establish the equations of motion for the cable in the literature. In this paper, we employ Newton's second law to derive the equations of motion for a flexible and elastic cable.

In previous studies of towed cable systems, experimental results were used to validate the mathematical model in the simulation [14–19]. Cochran et al. [15] experimentally validated the theoretical model in a wind tunnel by comparing the lateral motions of the towed body in both experimental and simulation results. Short cables (1.5 – 3 m) and different wind speed conditions were used. Borst et al. [16] compared the drogue altitude and tension forces in flight test and simulation results in which the towing plane flew in an orbital path and a five mile long cable was used. Hover [17] conducted the experiment in a test tank using a 1000 m long cable to study the control strategy of dynamic positioning of a towed pipe under water. Clifton et al. [18] conducted a flight test by commanding the towing plane on a circular path using a 20,000 ft long cable connected to the drogue. The drogue altitude variations were compared between flight test and simulation results. Williams et al. [14] presented experimental results using a rotated arm in a water tank

towing different types of cable. Additional measurements were also taken using a 3 m long cable attached to a ceiling fan spinning at 72 rpm.

The experiments presented in the literature were conducted either using short cables, less than 10 m [14, 15], or long cables, more than 1000 m [16–18], and aerial towed cable systems are typically steered by manned aircraft, which make the experiments very expensive and difficult to execute and repeat. In our previous work [19], an unmanned towing vehicle and 100 m long cable were used to collect data for model validation. The purpose was to determine aerodynamic lift and drag coefficients for the drogue in the simulation by using the model of a single-link cable. In this paper, we extend our work in model validation by comparing trajectories of the drogue in flight test with those in simulations using models with different numbers of cable links. Increasing the number of cable links in the model leads to a more realistic representation of cable dynamics but also increases the computational burden. One of the objectives of this paper is to determine the number of cable links that leads to a sufficiently accurate model while allowing efficient optimal trajectory generation of the mothership.

Given a mathematical model with sufficient fidelity, we need a strategy to regulate the mothership motion so that the drogue trajectory follows a desired path. Existing methods for generating the desired trajectory for the mothership can be classified into two categories: differential flatness based methods [11, 20–23] and optimal control based methods [6, 9, 13, 24–26].

Murray [11] presented a differential flatness based solution in which the motion of the system was parametrized using the motion of the towed-body as a flat output. However, Murray’s solution technique had numerical stability problems and was not further developed. A similar scheme of using differential flatness for motion planning of the mothership was discussed by Williams [20]. In our previous work, we applied differential flatness to generate the desired trajectory for the mothership and develop a nonlinear control law for the mothership based on its dynamic model in the presence of wind disturbances [21, 22]. The differential flatness based method is typically applied to the discretized model of the cable, and is computationally inexpensive compared to the optimal control methods. However it requires the equations of motion of the system to be differentially flat [27]. Another limitation is that this method does not take the performance limitations of the system

into consideration, so that the resulting trajectory of the towing vehicle might be impractical. In particular, the resulting trajectories may violate constraint limits on the manipulated variables (e.g. maximum available mothership thrust) or the controlled variables (e.g. tension limitations of the cable).

Optimal control based methods were also used to generate the desired trajectory for the towing vehicle. Williams [6, 13] employed an optimal control method to find a periodic path for the towing vehicle in order to minimize the motion of the towed body subject to dynamic constraints. Sequential quadratic programming was used to solve the optimization problem. Williams et al. [7] used simulated annealing to solve the optimal control problem in scheduling the orbit radius of the towing vehicle while the system transitions from a straight flight into an orbit. Williams et al. [28] used optimal control in determining the motion of the towing plane, as well as the cable deployment rate so that the towed body passed through a set of desired waypoints. Williams [9] extended his work to find an optimal elliptical orbit and cable deployment rate to compensate for crosswind disturbances. Establishing an optimal motion of the towing vehicle subject to constraints using a discretized multi-link cable model is a complicated optimization problem with many states and degrees of freedom. However, discussions of the computational burden were seldom mentioned. The typical algorithm used in solving the problem are based on quadratic programming in which squared-error objectives are used. In this paper, an approach based on Model Predictive Control (MPC) using the  $L_1$ -norm and squared error objectives are introduced and applied to perform the optimal trajectory generation of the towing vehicle.

MPC has been widely used in industrial applications such as chemical plants and refineries [29] based on empirical linear models [29–31] obtained by system identification. Because many of these applications have either semi-batch characteristics or nonlinear behavior, the linear models are retrofitted with elements that approximate nonlinear control characteristics to ensure that the linear models are applicable over a wider range of operating conditions and disturbances. The linear models adapt with either time or as a function of the current state of the system. A more general form that is not dependent on model switching is collections of Differential and Algebraic Equations (DAEs) in open equation format. These equations may include equality or inequality constraints, integer

variables, and differential elements. To apply DAEs to nonlinear models, different approaches have been studied and implemented in the literature, including simultaneous methods [32], decomposition methods [33, 34], efficient nonlinear programming solvers [35], improved estimation techniques [36–39], and large-scale techniques for applications to industrial systems [40, 41]. The objective function used in the control optimization problems are typically based on a weighted squared error or an  $L_2$ -norm form.

One novel contribution of this paper is the employment of a new  $L_1$ -norm objective function in the optimal control problem. The  $L_1$ -norm form objective has a number of advantages over traditional squared-error or  $L_2$ -norm objectives, including less sensitivity to data outliers and better rejection of measurement noise. Many of the remaining challenges associated with implementing nonlinear models are due to the complexity of the numerical solution techniques. To meet this demand, commercial and academic software have been developed. APMonitor Modeling Language [42] is one of the software that aim to model and solve the large-scale DAEs. Many algorithms like filtered bias updating, Kalman filtering, Moving Horizon Estimation (MHE) and nonlinear MPC can be implemented in this web-services platform through interfaces to MATLAB or Python. In this paper, we use a nonlinear MPC method to solve the optimal trajectory generation problem in which the mothership with performance limits is maneuvered to place the towed drogue onto a desired orbit. A combined objective functions is utilized in which a squared-error form objective aims to calculate the trajectory tracking error and  $L_1$ -norm objectives are employed to regulate the constraints. The MPC algorithm is implemented using APMonitor Modeling Language.

The remainder of the paper is structured as follows. In Section II, the mathematical model of the cable-drogue system is established using a lumped mass approach and Newton’s second law is employed to derive the dynamic equations of the system. In Section III, the validation of the mathematical model with different number of cable links is conducted using flight test data. Section IV introduces the formulation of nonlinear MPC used to generate a constrained optimal trajectory for the mothership. Section V shows the numerical results of the optimal trajectory generation of the mothership using various desired drogue motions.

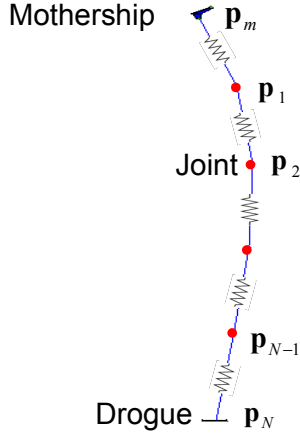


**Fig. 2** This figure shows the mothership-cable-drogue system in the simulation. The mothership ( $\mathbf{p}_m$ ) is modeled as a point mass. The cable is modeled as a finite number of point mass nodes ( $\mathbf{p}_1$  to  $\mathbf{p}_N$ ) connected by  $N$ -link springs. The drogue ( $\mathbf{p}_N$ ) is modeled as the last joint of the cable.

## II. Mathematical Model of the Cable-drogue System

The cable connecting the mothership and drogue can be modeled as an elastic or non-elastic flexible string. In the literature, the dynamics of towed-body systems were modeled by assuming that the cable is flexible and non-elastic [11, 15, 18, 43–45]. In our own flight tests, a fishing line was utilized as the cable and we have observed that the cable stretched considerably [19]. An elastic model for the cable is therefore needed in simulation to properly capture the dynamics of the system. In this section, we derive the cable-drogue dynamics using an elastic model. Figure 2 depicts a mothership-cable-drogue system with an  $N$ -link cable modeled as a finite number of point mass nodes connected by springs. The drogue is the last joint of the cable.

### A. Equations of Motion of the Cable-drogue System

In the system model, the position of the 0<sup>th</sup> joint of the cable  $\mathbf{p}_m \in \mathbb{R}^3$  is the position of the mothership;  $\mathbf{p}_j \in \mathbb{R}^3$ ,  $j = 1, 2, \dots, N$ , is the location of the  $j^{\text{th}}$  joint in the inertial frame;  $m_j$  is the mass of the  $j^{\text{th}}$  link;  $m_{dr}$  is the mass of the drogue;  $\mathbf{G}_j, \mathbf{F}_j^{aero} \in \mathbb{R}^3$  are the gravity and aerodynamic forces acting on the  $j^{\text{th}}$  link, respectively; and  $\mathbf{G}_{dr}, \mathbf{F}_{dr}^{aero} \in \mathbb{R}^3$  are the gravity and aerodynamic forces acting on the drogue, respectively. Let  $\ell_0 \triangleq L_0/N$  be the unstretched length of each link,

where  $L_0$  is the total unstretched length of the cable. The tension exerted on the  $j^{\text{th}}$  mass by the  $(j-1)^{\text{th}}$  mass is given by

$$\mathbf{T}_j = \frac{EA}{\ell_0} (\|\mathbf{p}_{j-1} - \mathbf{p}_j\| - \ell_0) \frac{\mathbf{p}_{j-1} - \mathbf{p}_j}{\|\mathbf{p}_{j-1} - \mathbf{p}_j\|},$$

where  $E$  is the Young's modulus and  $A$  is the cross-sectional area of the cable.

From Newton's second law, the equations of motion of the  $j^{\text{th}}$  cable joint and the drogue are given by

$$m_j \ddot{\mathbf{p}}_j = \mathbf{T}_j + \mathbf{G}_j + \mathbf{F}_j^{\text{aero}} - \mathbf{T}_{j+1}, \quad j = 1, 2, \dots, N-1,$$

$$(m_N + m_{dr}) \ddot{\mathbf{p}}_N = \mathbf{T}_N + \mathbf{G}_N + \mathbf{F}_N^{\text{aero}} + \mathbf{G}_{dr} + \mathbf{F}_{dr}^{\text{aero}}.$$

## B. Applied Forces on the Cable-drogue System

The applied forces on each joint consists of gravity and aerodynamic forces.

### 1. Gravity

Letting  $\mathbf{e}_3 \triangleq (0, 0, 1)^T$  be a unit vector in North-East-Down (NED) coordinates, and let  $g$  be the gravitational force exerted on a unit mass at Earth sea level, then the gravity forces exerted on the  $j^{\text{th}}$  joint and drogue are given by

$$\mathbf{G}_j = m_j g \mathbf{e}_3, \quad \text{and} \quad \mathbf{G}_{dr} = m_{dr} g \mathbf{e}_3. \quad (1)$$

### 2. Aerodynamic Forces of the Cable

The aerodynamic forces acting on the cable can be determined based on the cross-flow principle described in [6, 15]. Any components of the forces due to effects such as vortex shedding are not treated in the model. Letting  $\mathbf{l}_j \triangleq \mathbf{p}_{j-1} - \mathbf{p}_j$ ,  $j = 1, 2, \dots, N$ , be the position vector between the  $(j-1)^{\text{th}}$  and  $j^{\text{th}}$  joints, the corresponding lift and drag forces are calculated using  $\mathbf{v}_j^s$ , the velocity vector of the  $j^{\text{th}}$  cable link relative to the wind frame, which can be approximated from the motion of the adjacent joints as

$$\mathbf{v}_j^s = \frac{1}{2} [(\dot{\mathbf{p}}_{j-1} - \mathbf{w}_c) + (\dot{\mathbf{p}}_j - \mathbf{w}_c)],$$

where  $\mathbf{w}_c$  is the constant component of the wind expressed in the inertial frame. The angle of attack of the  $j^{\text{th}}$  link  $\alpha_j$  can be computed as

$$\alpha_j = \cos^{-1} \frac{\mathbf{l}_j \cdot \mathbf{v}_j^s}{\|\mathbf{l}_j\| \|\mathbf{v}_j^s\|}. \quad (2)$$

Letting  $M_{p_j}$  be the Mach number parallel to the  $j^{\text{th}}$  link, and  $M_{n_j}$  be the Mach number normal to the  $j^{\text{th}}$  link, the drag and lift coefficients of the  $j^{\text{th}}$  link are given by [6, 15]

$$C_{D_j} = C_{f_j} + C_{n_j} \sin^3 \alpha_j, \quad (3)$$

$$C_{L_j} = C_{n_j} \sin^2 \alpha_j \cos \alpha_j, \quad (4)$$

where

$$C_{f_j} = \begin{cases} 0.038 - 0.0425 M_{p_j} & M_{p_j} < 0.4 \\ 0.013 + 0.0395 (M_{p_j} - 0.85)^2 & M_{p_j} \geq 0.4 \end{cases} \quad (5)$$

$$C_{n_j} = 1.17 + M_{n_j}/40 - M_{n_j}^2/4 + 5M_{n_j}^3/8 \quad (6)$$

The unit vectors defining the directions of the drag and lift forces in the inertial frame are

$$\mathbf{e}_{D_j} = -\frac{\mathbf{v}_j^s}{\|\mathbf{v}_j^s\|}, \quad (7)$$

$$\mathbf{e}_{L_j} = -\frac{(\mathbf{v}_j^s \times \mathbf{l}_j) \times \mathbf{v}_j^s}{\|(\mathbf{v}_j^s \times \mathbf{l}_j) \times \mathbf{v}_j^s\|}, \quad (8)$$

where  $\times$  denotes the cross product of two vectors. Letting  $\rho$  be the atmospheric density,  $\ell_j$  be the stretched length of the  $j^{\text{th}}$  cable link, and  $d$  be the diameter of the cable link, the drag and lift forces acting on the  $j^{\text{th}}$  link are given by

$$\mathbf{D}_j = \frac{1}{2} \rho C_{D_j} \ell_j d \|\mathbf{v}_j^s\|^2 \mathbf{e}_{D_j}, \quad (9)$$

$$\mathbf{L}_j = \frac{1}{2} \rho C_{L_j} \ell_j d \|\mathbf{v}_j^s\|^2 \mathbf{e}_{L_j}. \quad (10)$$

These lift and drag vectors are assumed to be constant over each cable link. Hence the aerodynamic forces are lumped and centered at the midpoint of the link. The aerodynamic forces exerted on the  $j^{\text{th}}$  joint are given by

$$\mathbf{F}_j^{aero} = \frac{1}{2} [(\mathbf{D}_j + \mathbf{D}_{j+1}) + (\mathbf{L}_j + \mathbf{L}_{j+1})], \quad j = 1, 2, \dots, N-1.$$

The aerodynamic force exerted on the drogue from the last link of the cable is

$$\mathbf{F}_N^{aero} = \frac{1}{2} (\mathbf{D}_N + \mathbf{L}_N).$$

### 3. Aerodynamic Forces of the Drogue

Letting  $C_{L_{dr}}$  and  $C_{D_{dr}}$  be the aerodynamic lift and drag coefficients of the drogue, respectively,  $S_{dr}$  be the planform area of the drogue wing,  $\mathbf{v}_{dr}^s$  be the velocity vector of the drogue relative to the wind frame,  $\mathbf{e}_{L_{dr}}$  be the unit vector representing the direction of the aerodynamic lift force on the drogue, the aerodynamic lift and drag forces on the drogue are given by

$$\mathbf{L}_{dr} = \frac{1}{2} \rho C_{L_{dr}} S_{dr} \|\mathbf{v}_{dr}^s\|^2 \mathbf{e}_{L_{dr}},$$

$$\mathbf{D}_{dr} = -\frac{1}{2} \rho C_{D_{dr}} S_{dr} \|\mathbf{v}_{dr}^s\| \mathbf{v}_{dr}^s,$$

where

$$\mathbf{e}_{L_{dr}} = -\frac{(\mathbf{v}_{dr}^s \times \mathbf{e}_3) \times \mathbf{v}_{dr}^s}{\|(\mathbf{v}_{dr}^s \times \mathbf{e}_3) \times \mathbf{v}_{dr}^s\|}.$$

## III. Validation of the Mathematical Model using Experimental Data

In this section, the fidelity of the mathematical model developed in the previous section is validated with flight test data. Because the number of cable links used in the simulation determines the complexity of the equations of motion of the cable, and affects the computation time in the optimization algorithms, in this section, we will focus on determining an appropriate number of cable links that strikes a compromise between the accuracy and complexity of the cable mathematical model.

### A. Hardware System Description

The hardware system used to collect experimental data consisted of four elements – a mothership UAS, a hemisphere-shaped drogue, a 100 m long cable and a ground station. The key parameters of the systems are shown in Table 1.

**Table 1 System parameters in flight test**

Mothership		Drogue		Cable	
Mass (kg)	1.76	Mass (kg)	0.32	Mass (kg)	0.02
$C_L$	0.28	Wing area (m <sup>2</sup> )	0.055	Length (m)	85
$C_D$	0.06	$C_L$	0.01	$E$ (GPa)	1.9
Wing area (m <sup>2</sup> )	0.307	$C_D$	0.42	$d$ (mm)	0.46
Wing span (m)	1.4	Diameter (m)	0.3		

The mothership, shown in Fig. 3 (a), was a fixed wing UAS with two 770 Watt battery-operated motors, and was equipped with a Kestrel 2 autopilot, shown in Fig. 3 (d), and a radio modem to communicate with the ground station. To prevent the cable and drogue from exerting large forces during the landing phase, a cable release module was placed on the underside of the mothership, and was actuated from the ground station. The hemisphere-shaped drogue with 30-cm diameter used in the flight test was constructed of reinforced plastic, as shown in Fig. 3 (b). The drogue was equipped with a Kestrel 2 autopilot and radio modem for reporting its position and velocity to the ground station. The cable is a trichloroethylene fishing line, with 0.46 mm diameter and 20 lb maximal load, and the mass of a 100 m cable is approximate 20 g. The ground station consists of a desktop computer with Intel *i5* processor running at 3.1 GHz with 8 GB RAM, a radio modem combobox, and a remote controller. The ground station control software was Virtual Cockpit (VC), developed by Procerus Technologies.

## B. Flight Test

In the flight test, the mothership was commanded to follow a loiter of 100 m radius and a constant altitude of 125 m with the airspeed commanded at 14 m/s. The results of the system trajectory are shown in Fig. 4. The top-down view of the system trajectory presented in Fig. 4 (a) shows that a circular mothership orbit resulted in a smaller circular orbit of the drogue. Because of the wind, the center of the drogue orbit shifted to the west. The East-Altitude view of the system trajectory presented in Fig. 4 (b) shows that the resulting drogue orbit was inclined because of the wind. The amplitude of the drogue's altitude oscillation was approximately 20 m. The onboard



(a) Mothership with 1.4 m wing span, twin props and cable release mechanism.



(b) Hemisphere-shaped drogue with 30 cm diameter made of reinforced plastic.



(c) Fishing line cable with 20 lb maximal payload.



(d) Kestrel 2 autopilot developed by Procerus Technologies.

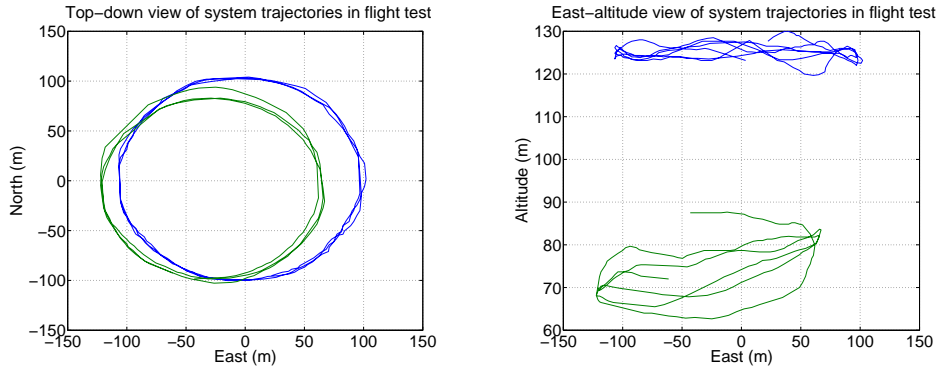
**Fig. 3 Hardware systems used in flight test.**

measurement of GPS velocities of the mothership and drogue, the airspeed of the mothership are shown in Fig. 5 (a). It can be seen that the actual airspeed of the mothership essentially followed the commanded value, and the GPS velocities of the mothership and drogue oscillated between 8 m/s and 20 m/s, which implies the average wind was approximately 6 m/s. Figure 5 (b) shows the wind estimation in the north and east directions, respectively. The direction of the wind matched the direction of the center shift of the drogue orbit, while the average magnitude of the wind (approximately 4 m/s) was smaller than the one implied in Fig. 5 (a). The difference may come from the GPS drifting error or the wind estimation error.

### C. Model Validation

To validate the mathematical model, we force the simulated mothership to follow the same trajectory as the actual mothership, and then compare the motion of the simulated drogue to the motion of the actual drogue. The number of links in the cable are increased until a suitable match is obtained.

Using the parameters shown in Table 1, we conducted simulations using different numbers of

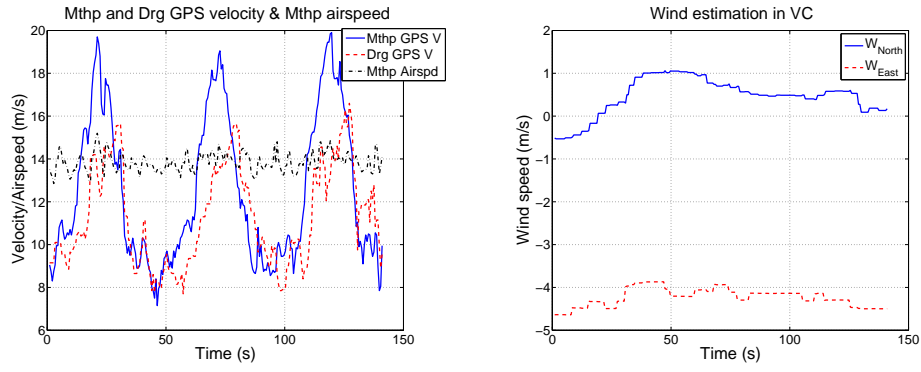


(a) Top-down view of the orbits of the mothership and drogue in flight test. The mothership (larger) orbit was commanded with a radius of 100 m and airspeed of 14 m/s. The drogue (smaller) orbit had a resulting radius of approximately 90 m. The center of the drogue orbit shifted to the west of the center of the mothership orbit due to the wind.

(b) Side (East-altitude) view of the orbits of the mothership and drogue during flight test. The mothership (upper) orbit was essentially horizontal, while the drogue (lower) orbit is inclined due to the wind. The amplitude of the drogue's altitude oscillation was approximately 20 m.

**Fig. 4 Trajectories of the mothership and drogue in the flight test.**

cable links. The airspeed of the mothership was selected as 14 m/s and the constant wind vector was selected as  $(0.5 - 4)$  m/s in the North-East coordinate. Figure 6 overlays the mothership trajectories from both flight test and simulation in north, east and altitude directions, respectively. It can be seen that the trajectory of the simulated mothership essentially matched the trajectory of the actual mothership during the flight test. Figure 7 shows the trajectories of the simulated drogue using 1, 2 and 5 cable links, respectively, overlaid on the trajectory of the actual drogue during flight test. It can be seen that in the north and east directions, the simulation results essentially match the flight test results. In the altitude direction, as the number of cable links increased, the simulation results followed the flight results more accurately in terms of phase, but the amplitude of the oscillation slightly decreased. Figure 8 shows the top-down and side views of the drogue trajectories from both simulation and the flight test. It can be seen from Figs. 7 and 8 that as the number of cable links increases, the radii of simulated drogue orbits increased which match the real drogue orbit more precisely, while the amplitudes of simulated drogue's altitude oscillations



(a) This figure shows the mothership airspeed (dash-dot line) essentially followed the commanded value (14 m/s), and the GPS velocities (ground speed) of the mothership (solid line) and drogue (dashed line) oscillated between 8 m/s and 20 m/s, which implies the wind was approximately 6 m/s.

(b) Wind estimation in North (solid line) and East (dashed line) directions. The direction of the wind matched the direction of the center shift of the drogue orbit, and the average magnitude of the wind was approximately 4 m/s.

**Fig. 5 Measurements obtained from Virtual Cockpit.**

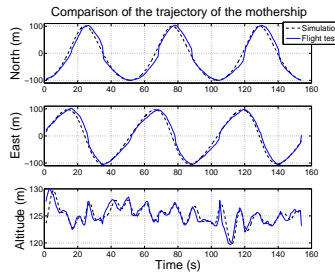
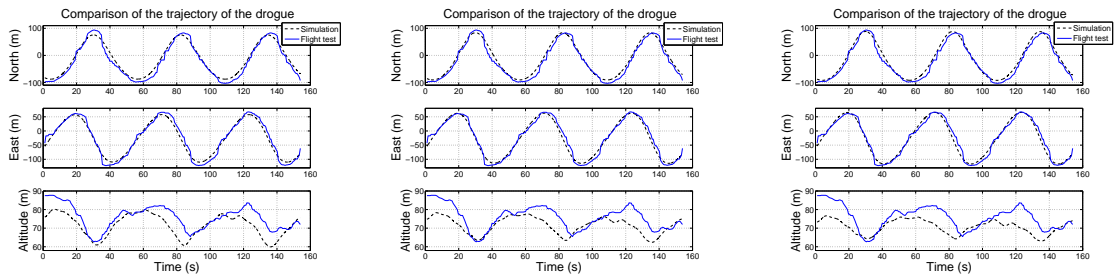


**Fig. 6 This figure shows that the mothership trajectory of the simulation (dashed line) essentially followed the trajectory of the flight test (solid line) in three dimensions.**

decreased which deviate from the flight test result. Thus, it can be seen that simulations with 1 to 5 cable links verified that an increased number of cable links did not significantly improve the accuracy of the predictions. As a compromise between the accuracy of the simulation model and the computational burden of the successive optimal trajectory generation, we selected  $N = 2$  as the number of cable link in the equations of motion.



(a) Results using 1-link cable.

(b) Results using 2-link cable.

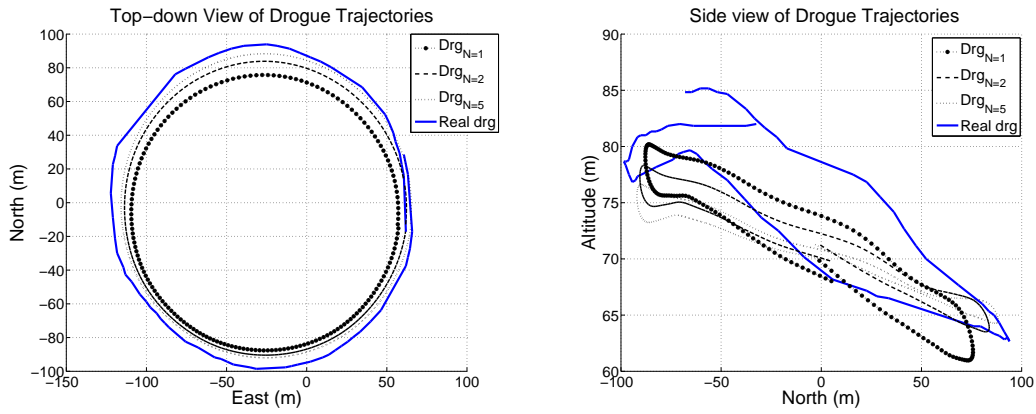
(c) Results using 5-link cable.

**Fig. 7 Comparison of the drogue trajectories in the flight test (solid line) and simulation (dashed line) using a different number of cable links in north, east and altitude directions, respectively. In the north and east directions, the simulation trajectories essentially matched the flight test results. In the altitude direction, as the number of cable links increased, the simulation results followed the flight test results more accurately in terms of phase, while the amplitude of the altitude oscillation slightly decreased.**

#### IV. MPC Formulation

Given a desired trajectory for the drogue (e.g., a level circular orbit), a strategy is needed to generate a mothership trajectory that produces the desired drogue path. Differential flatness has been used in the trajectory generation of the towed cable system in [11, 20–22] by applying certain types of dynamic models of the cable. For the mathematical model presented in Section II, it is nontrivial to calculate the desired mothership trajectory by using differential flatness. In addition, since the mothership has performance limits like airspeed, roll angle, and climbing rate, differential flatness based methods do not directly take these constraints into consideration. Furthermore, during transitions between straight and level flight and orbital flight, the tension forces exerted on the cable should not exceed the loading limit of the cable.

In this section, a strategy is developed to produce an optimal trajectory for the mothership to place the drogue onto the desired orbit in the presence of system constraints. In the literature, when formulating the optimal control problem for generating the desired mothership trajectory, the nonlinear kinematic or dynamic models of the mothership were typically used, and the objective functions were usually based on squared error or  $L_2$ -norm form. In this section, to reduce the computation time, we use linear dynamic equations of the mothership and a novel format of the



(a) Top-down view of drogue trajectories using different number of cable links in the simulation and flight test. As the number of cable links increased, the radius of the drogue orbit increased.

(b) Side view of drogue trajectories using different number of cable links in the simulation and flight test. As the number of cable links increased, the amplitude of the altitude oscillation slightly decreased.

**Fig. 8 Drogue trajectories in the flight test (solid line) and simulation using a different number of cable links (star-dot line for the 1-link model, dashed line for the 2-link model and dotted line for the 5-link model).**

objective function to formulate the MPC problem.

Letting  $\mathbf{v}_m \in \mathbb{R}^3$  be the mothership velocity relative to the wind frame and  $\mathbf{a}_m \in \mathbb{R}^3$  be the mothership acceleration in the inertial frame, which is selected as the input of the mothership dynamic, the equations of motion for the mothership are given by

$$\dot{\mathbf{p}}_m = \mathbf{v}_m + \mathbf{w}_c \quad (11)$$

$$\dot{\mathbf{v}}_m = \mathbf{a}_m. \quad (12)$$

The performance constraints of the mothership are typically given by the magnitude of the mothership airspeed  $V_a$ , the heading angle  $\psi$ , the bank angle  $\phi$ , and the air mass referenced flight path angle  $\gamma_a$ , which is defined as the angle from the inertial North-East plane to the velocity vector of the aircraft relative to the air mass. The kinematic equations of motion for the mothership are

written as

$$\dot{p}_n = V_a \cos \psi \cos \gamma_a + w_n \quad (13)$$

$$\dot{p}_e = V_a \sin \psi \cos \gamma_a + w_e \quad (14)$$

$$\dot{p}_d = -V_a \sin \gamma_a + w_d \quad (15)$$

$$\dot{\psi} = \frac{g}{V_a} \tan \phi. \quad (16)$$

By comparing Eqs. (11) and (12), the constrained variables can be expressed as

$$\begin{aligned} V_a &= \|\mathbf{v}_m\| \\ \psi &= \tan^{-1} \left( \frac{\mathbf{v}_m(2)}{\mathbf{v}_m(1)} \right) \\ \gamma_a &= -\sin^{-1} \left( \frac{\mathbf{v}_m(3)}{V_a} \right) \\ \dot{\psi} &= \frac{\mathbf{a}_m(2) \mathbf{v}_m(1) - \mathbf{a}_m(1) \mathbf{v}_m(2)}{\|\mathbf{v}_m\|^2} \\ \phi &= \tan^{-1} \left( \frac{V_a}{g} \dot{\psi} \right). \end{aligned}$$

Letting  $\mathbf{p}_{dr}^d(t) \in \mathbb{R}^3$  be the desired drogue trajectory,  $\mathbf{p}_{dr}(t) \in \mathbb{R}^3$  be the actual drogue trajectory,  $\Phi \in \mathbb{R}$  be the objective function value,  $\mathbf{y} \triangleq (y_0, \dots, y_n)^T \in \mathbb{R}^n$  be the controlled variables,  $\mathbf{y}_{hi}, \mathbf{y}_{lo} \in \mathbb{R}^n$  be the higher and lower dead-bands of the controlled variables,  $\mathbf{w}_{hi}, \mathbf{w}_{lo} \in \mathbb{R}^n$  be the weights on the controlled variables outside the dead-bands,  $\mathbf{u} \in \mathbb{R}^n$  be the inputs,  $\mathbf{c}_y, \mathbf{c}_u \in \mathbb{R}^n$  are cost weights of  $\mathbf{y}$  and  $\mathbf{u}$ ,  $\mathbf{f} : \mathbb{R}^n \rightarrow \mathbb{R}^n$  represent the equations of motion,  $\mathbf{x} \in \mathbb{R}^n$  be the states of the equations of motion,  $\mathbf{d} \in \mathbb{R}^n$  be parameters or unmeasured disturbances,  $\mathbf{g}_{iec} : \mathbb{R}^n \rightarrow \mathbb{R}^n$  represent the inequality constraints,  $\tau \in \mathbb{R}$  be the response time constant of the desired controlled variables,  $\mathbf{sp}_{hi}, \mathbf{sp}_{lo} \in \mathbb{R}^n$  be dead-band setpoints, and  $\mathbf{e}_{hi}$  and  $\mathbf{e}_{lo}$  be slack variables [47] selected by the optimizer to penalize  $\mathbf{y}$  above and below the dead-band, and given by

$$\mathbf{e}_{hi,i} = \begin{cases} \mathbf{y}_i - \mathbf{y}_{hi,i} & \mathbf{y}_i - \mathbf{y}_{hi,i} \geq 0 \\ 0 & \mathbf{y}_i - \mathbf{y}_{hi,i} < 0 \end{cases} \quad \text{and} \quad \mathbf{e}_{lo,i} = \begin{cases} \mathbf{y}_{lo,i} - \mathbf{y}_i & \mathbf{y}_{lo,i} - \mathbf{y}_i \geq 0 \\ 0 & \mathbf{y}_{lo,i} - \mathbf{y}_i < 0 \end{cases}, \quad i = 1, \dots, n,$$

then the trajectory generation problem can be posed as the following optimization problem:

$$\begin{aligned} \min_{\mathbf{u}(t_0, t_1)} \Phi &= \mathbf{w}_{hi}^T \mathbf{e}_{hi} + \mathbf{w}_{lo}^T \mathbf{e}_{lo} + \mathbf{y}^T \mathbf{c}_y + \mathbf{u}^T \mathbf{c}_u \\ &+ \int_{t_0}^{t_1} (\mathbf{p}_{dr}(\delta) - \mathbf{p}_{dr}^d(\delta))^T (\mathbf{p}_{dr}(\delta) - \mathbf{p}_{dr}^d(\delta)) d\delta \end{aligned} \quad (17a)$$

$$\text{s.t. } \mathbf{f}(\dot{\mathbf{x}}, \mathbf{x}, \mathbf{y}, \mathbf{u}, \mathbf{d}) = \mathbf{0} \quad (17b)$$

$$\mathbf{g}_{iec}(\dot{\mathbf{x}}, \mathbf{x}, \mathbf{y}, \mathbf{u}, \mathbf{d}) \geq \mathbf{0} \quad (17c)$$

$$\tau \frac{\partial \mathbf{y}_{hi}}{\partial t} + \mathbf{y}_{hi} = \mathbf{sp}_{hi} \quad (17d)$$

$$\tau \frac{\partial \mathbf{y}_{lo}}{\partial t} + \mathbf{y}_{lo} = \mathbf{sp}_{lo}. \quad (17e)$$

A combination of  $L_1$ -norm and squared-error objectives, shown in Eq. (17a), is used to accomplish multiple objectives. The controlled variables  $y$  are selected as the constraints of the system. The  $L_1$ -norm objective was used to regulate high-priority constraints like the cable tension and the airspeed of the mothership. In this case, the controlled variables were not forced to follow a desired trajectory, but were constrained to remain within certain range of acceptable limits. The slack variables  $\mathbf{e}_{hi}$  and  $\mathbf{e}_{lo}$  are then used to regulate  $\mathbf{y}$  to remain within dynamic dead-bands parametrized by  $\mathbf{y}_{hi}$  and  $\mathbf{y}_{lo}$ . The squared-error (integration) term was used to penalize the trajectory tracking error of the drogue with a lower weighting that represented the lower priority of the tracking objective. Eqs. (17b) and (17c) are used to regulate the states to satisfy the equations of motion and inequality constraints.

Eqs. (17d) and (17e) are linear first order equations that define the regulations for controlled variables represented by either a dead-band or reference trajectory to the setpoints. The setpoints  $\mathbf{sp}_{hi}$  and  $\mathbf{sp}_{lo}$  are used to define regions that are not penalized in the objective function and are referred to as the "dead-band". It is desirable to make the evolution of the controlled variables effectively approach setpoints at a specified rate so that excessive movements of manipulated variables or response overshoots of controlled variables can be avoided. Based on different control objectives, the initial conditions of  $\mathbf{y}_{hi}$  and  $\mathbf{y}_{lo}$ , can be set to give a wider dead-band at the beginning of the simulation and only to enforce the steady state response (and vice versa). Different initial conditions defining a wide or narrow dead-band are the trade-off between precise steady-state response and

precise dynamic evolution. Therefore, reference trajectories of  $\mathbf{y}$  by specifying the values of  $\mathbf{sp}_{hi}$  and  $\mathbf{sp}_{lo}$  can be a step, ramp or other dynamic signals.

## V. Numerical Results

In this section, the MPC based approach described in Section IV is employed to compute open-loop mothership trajectories for a variety of desired drogue trajectories. The performance limits of the mothership are selected as  $\dot{\psi} \in [-0.35, 0.35]$  rad/s,  $V_a \in [10, 20]$  m/s and  $\gamma_a \in [-0.35, 0.35]$  rad. The MPC problem was solved using APMonitor Modeling Language [42]. A step size of 2 seconds was selected as a compromise between the computation time and the accuracy of the results. The computer used to solve the optimization problem has an AMD 64 core processor with 64 GB of RAM.

### A. Desired Drogue Orbit with Constant Ground Speed

In the final phase of the aerial recovery scenario, the drogue must be placed onto an orbit that can be easily followed by the MAV. In this section, the desired drogue trajectory is a circular orbit with constant altitude and constant ground speed. Let  $r_{dr}^d$  be the desired constant orbit radius of the drogue,  $\theta(t)$  be the orbital angle of the orbit measured from North, and  $h_0$  be the desired constant altitude of the drogue, the desired circular orbit of the drogue in three dimensions is given by

$$p_{dr_n}^d(t) = r_{dr}^d \cos \theta(t) \quad (18)$$

$$p_{dr_e}^d(t) = r_{dr}^d \sin \theta(t) \quad (19)$$

$$p_{dr_d}^d(t) = -h_0. \quad (20)$$

Letting  $v_{dr}^g$  be the desired constant ground speed of the drogue, the orbit angle for a clockwise motion can be written as  $\theta(t) = v_{dr}^g t / r_{dr}$ . Without loss of generality, the wind is assumed from the west. A typical circular orbit for drogue can be parametrized by selecting  $v_{dr}^g = 12$  m/s,  $h_0 = 100$  m and  $r_{dr}^d = 100$  m. Then the orbit period can be calculated by  $T_p^g = 2\pi r_{dr}^d / v_{dr}^g = 52.36$  s. The starting and ending times are selected as  $t_0 = 0$  and  $t_1 = 70$  s, so that the resulting mothership trajectory has enough waypoints to produce an orbit. The optimal control solver is selected as IPOPT [46],

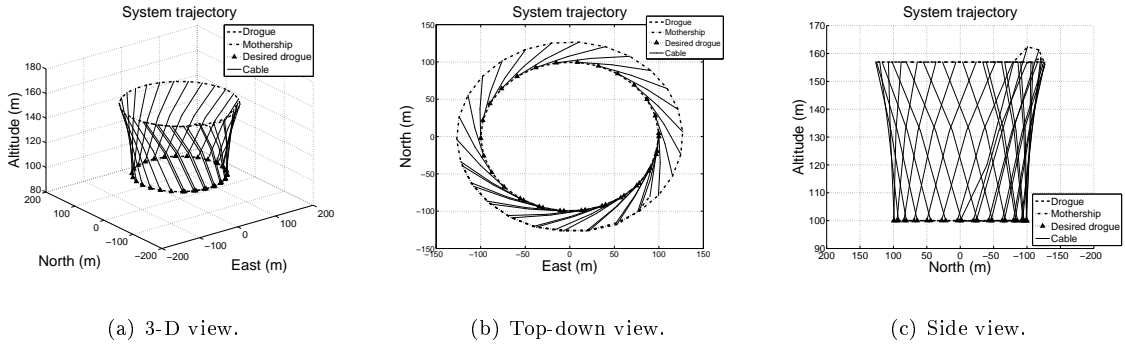


**Fig. 9** Optimal system trajectories in the absence of wind. A horizontally flat desired drogue orbit (triangle-dot line) requires a desired horizontally flat mothership orbit (dash-dot line). The actual drogue trajectory (dashed line) follows the desired orbit precisely. The cable (solid line) curved because of the aerodynamic forces exerted on the joint.

which is an open-source Interior Point solver for solving Nonlinear Programming (NLP) problems included with the COIN-OR collection. The initial configuration and solution results are shown in Table 2. It can be seen that the objective function values were less than 0.5 when the wind speeds were less than 5 m/s, and increased to approximately 8000 when the wind speed increased to 10 m/s. This is because the existing performance limits of the mothership made the resulting optimal orbit unable to precisely place the drogue orbit onto the desired orbit.

**Table 2** Solution results using the desired drogue orbit with constant ground speed

Wind speed (m/s)	$\mathbf{p}_m^0$ (m)	$\mathbf{v}_m^0$ (m/s)	Solution Time (s)	$\Phi$
0	(-79, 90, -157)	(-10, -8, 0)	18.4	0.1
$(0, 5, 0)^T$	(-67, 55, -157)	(-9.4, -7.3, 2)	17.1	0.2
$(0, 10, 0)^T$	(-61, 35, -142)	(-9, -5, 2)	48.1	7965.1
$\mathbf{p}_m^0$ = initial mothership position; $\mathbf{v}_m^0$ = initial mothership velocity in NED frame.				

Figure 9 shows the different views of optimal system trajectories in the absence of wind. It can be seen that a horizontally flat desired drogue orbit requires a desired horizontally flat mothership orbit. Figure 10 shows the different views of the optimal system trajectories in the presence of 5 m/s wind from the west. It can be seen that the desired mothership orbit is inclined to produce a horizontally flat orbit of the drogue in the presence of wind. The amplitude of the mothership's altitude oscillation was approximately 40 m. Figure 11 shows the evolutions of the constraints

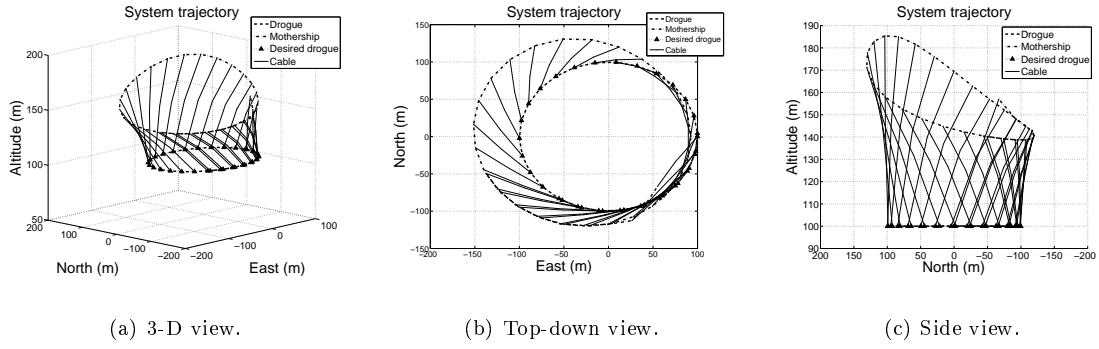


**Fig. 10** Optimal system trajectories using a desired drogue orbit with constant ground speed in the presence of 5 m/s wind from the west. A horizontally flat desired drogue orbit (triangle-dot line) resulted in an inclined desired mothership orbit (dash-dot line). The center of the mothership orbit shifted to the west of the center of the drogue orbit. The amplitude of the mothership's altitude oscillation was approximately 40 m.

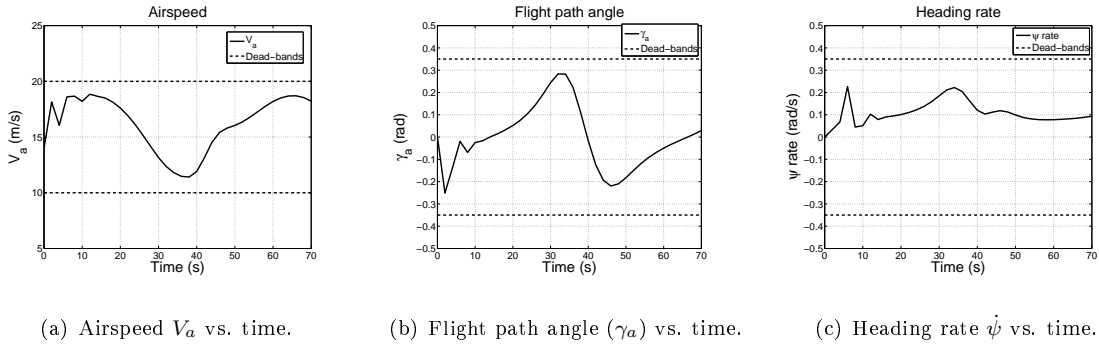


**Fig. 11** Evolution of constrained variables of the mothership using a desired drogue orbit with constant ground speed in the presence of 5 m/s wind from the west. All the variable values (solid lines) remained within their limits (dashed lines).

variables  $V_a$ ,  $\gamma_a$  and  $\dot{\psi}$  of the mothership. It can be seen that all the variables remained within the constraints. Figure 12 shows the different views of the optimal system trajectories in the presence of 10 m/s wind from the west. It can be seen that the desired mothership orbit inclines more in a stronger wind. Because of the performance limits of the mothership, the resulting optimal orbit was unable to precisely place the drogue orbit onto the desired orbit, which results in a large value for the objective function in Table 2. The amplitude of the mothership's altitude oscillation was approximately 70 m, while the amplitude of the drogue's altitude oscillation was approximately 15 m. Figure 13 shows the evolutions of the constraints  $V_a$ ,  $\gamma_a$  and  $\dot{\psi}$  of the mothership. It can be seen that although all the constrained variables reached their limits during the flight, the optimizer

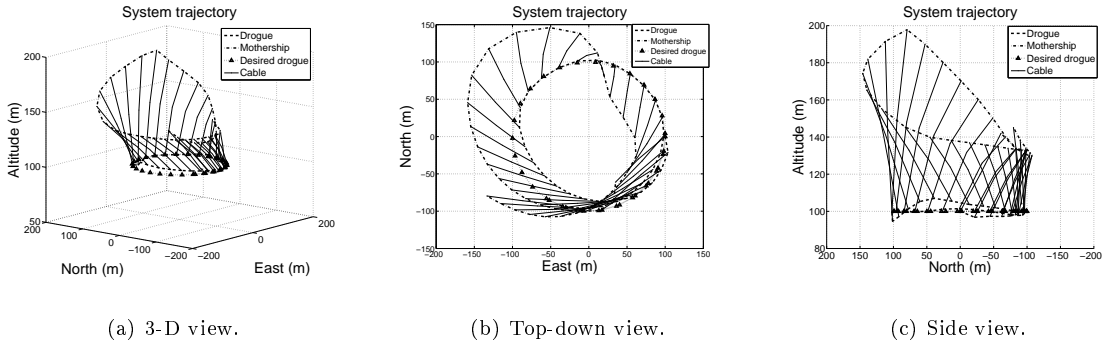


**Fig. 12** Optimal system trajectories using a desired drogue orbit with constant ground speed in the presence of 10 m/s wind from the west. The resulting optimal mothership orbit (dash-dot line) was unable to place the actual drogue trajectory (dashed line) onto the desired orbit (triangle-dot line) precisely because of the performance limits. The amplitude of the mothership’s altitude oscillation was approximately 70 m, while the amplitude of the drogue’s altitude oscillation was approximately 15 m.

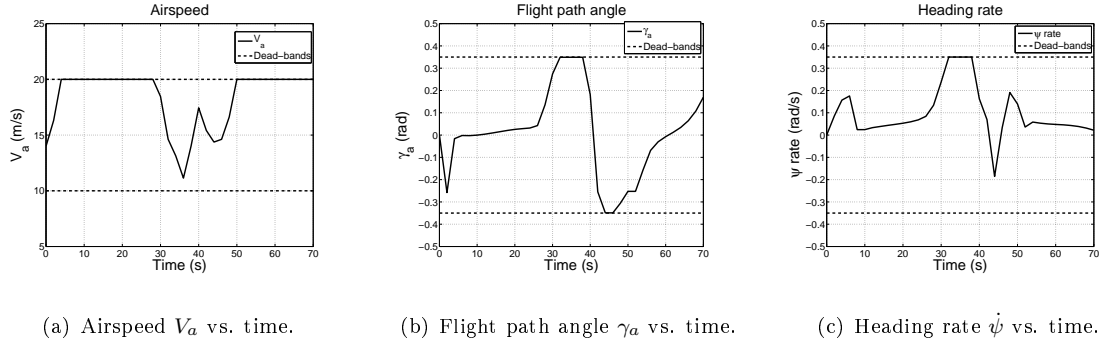


**Fig. 13** Evolution of constrained variables of the mothership using a desired drogue orbit with constant ground speed in the presence of 10 m/s wind from the west. All variables (solid lines) reached the limits (dashed lines) during the simulation. The optimizer was able to produce an optimal trajectory for the mothership by keeping all the constrained variables within their limits.

was able to produce an optimal trajectory for the mothership to place the drogue orbit to essentially follow the desired orbit.

### B. Desired Drogue Orbit with Constant Airspeed

Because the autopilot on the MAV is typically designed to regulate a constant airspeed, in this section, a desired drogue trajectory with constant airspeed is used to calculate the desired

mothership orbit. The time derivative of  $\mathbf{p}_{dr}^d(t)$  using Eqs. (18) to (20) is given by

$$\dot{\mathbf{p}}_{dr}^d = \begin{pmatrix} -r_{dr}^d \dot{\theta} \sin \theta \\ r_{dr}^d \dot{\theta} \cos \theta \\ 0 \end{pmatrix} = \mathbf{v}_{dr}^s + \mathbf{w}. \quad (21)$$

Thus, the airspeed of the drogue  $\|\mathbf{v}_{dr}^s\|$  is calculated as

$$\|\mathbf{v}_{dr}^s\| = \sqrt{\left(-r_{dr}^d \dot{\theta} \sin \theta - w_n\right)^2 + \left(r_{dr}^d \dot{\theta} \cos \theta - w_e\right)^2 + w_d^2}.$$

Given a desired drogue airspeed  $v_{dr}^a$ , we have

$$r_{dr}^2 \dot{\theta}^2 + 2r_{dr} (w_n \sin \theta - w_e \cos \theta) \dot{\theta} + w_n^2 + w_e^2 + w_d^2 - (v_{dr}^a)^2 = 0.$$

Therefore, solving the quadratic equation for  $\dot{\theta}$ , the clockwise motion is given by

$$\dot{\theta} = \frac{w_e \cos \theta - w_n \sin \theta + \sqrt{(w_n \sin \theta - w_e \cos \theta)^2 - \left(w_n^2 + w_e^2 + w_d^2 - (v_{dr}^a)^2\right)}}{r_{dr}}. \quad (22)$$

The orbital period  $T_p^a$  can be calculated by [9]

$$T_p^a = \int_0^{2\pi} \frac{1}{\dot{\theta}} d\theta. \quad (23)$$

It is not difficult to see that  $T_p^a$  increases when the wind speed increases. In the presence of 5 m/s wind,  $T_p^a$  can be calculated as 60.51 s by using Eq. (23). When the wind increases to 10 m/s,  $T_p^a$  increases to 135.8 s. To guarantee that the optimal trajectory of the mothership has enough waypoints to produce an orbit, the starting and ending times are selected as  $t_0 = 0$  and  $t_1 = 70$  s for the case of 5 m/s wind, and  $t_1 = 150$  s for the case of 10 m/s wind. The initial configuration and solution results are shown in Table 3. It can be seen that when the wind speed increased to 10 m/s, the objective function value increased to 755.2. This is because the existing performance limits of the mothership made the resulting optimal orbit unable to precisely place the drogue orbit onto the desired orbit. The parameters of the desired drogue orbit were selected as  $r_{dr} = 100$  m and  $v_{dr}^a = 12$  m/s to compare the results with those in the previous section.

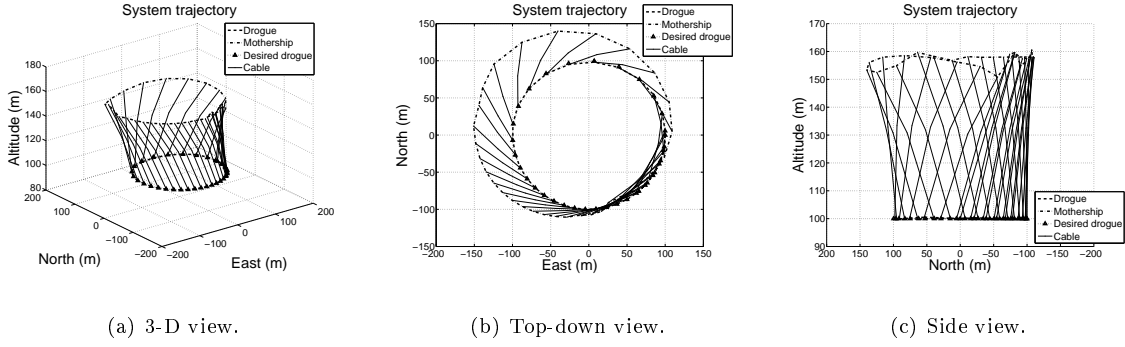


**Fig. 14** Optimal system trajectories using a desired drogue orbit with constant airspeed in the presence of 5 m/s wind from the west. The resulting optimal mothership orbit (dash-dot line) was larger than the one in Fig. 10. The amplitude of the mothership’s altitude oscillation was approximately 10 m, which was much smaller than the one in Fig. 10. The waypoints placed close together when the system was flying upwind (towards the west), and sparse when the system was flying downwind (towards the east).

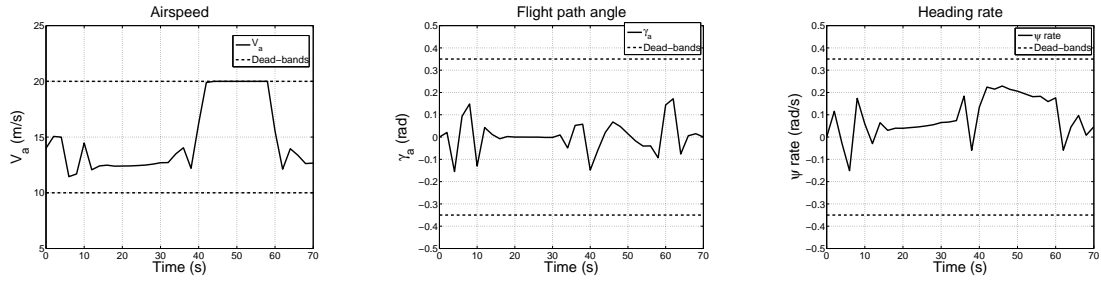
**Table 3** Solution results using the desired drogue orbit with constant airspeed

Wind speed (m/s)	$\mathbf{p}_m^0$ (m)	$\mathbf{v}_m^0$ (m/s)	Solution Time (s)	$\Phi$
$(0, 5, 0)^T$	$(-74, 63, -159)$	$(-6, -9, 0)$	18.8	17.9
$(0, 10, 0)^T$	$(-20, 40, -159)$	$(-3, -4, 0)$	39.8	755.2

$\mathbf{p}_m^0$  = initial mothership position;  $\mathbf{v}_m^0$  = initial mothership velocity in NED frame.

Figure 14 shows the different views of the optimal system trajectories in the presence of 5 m/s wind from the west. It can be seen that the offset of the mothership orbit center in Fig. 14 (b) is smaller than the one in Fig. 10 (b). It also can be seen that the inclination of the mothership orbit in Fig. 14 (c) was much smaller than the one in Fig. 10 (c). The amplitude of the mothership’s altitude oscillation was approximately 10 m. Because the desired airspeed of the drogue was constant, it can be seen that the waypoints placed close together when the system is flying upwind (towards the west), and sparsely when the system was flying downwind (towards the east). Figure 15 shows the evolutions of the constrained variables  $V_a$ ,  $\gamma_a$  and  $\dot{\psi}$  of the mothership. It can be seen that the desired airspeed of mothership in Fig. 15 (a) reached its upper limit, while in the same wind condition, the desired airspeed in Fig. 11 (a) was still within the limits.

Figure 16 shows the different views of the optimal system trajectories in the presence of 10 m/s

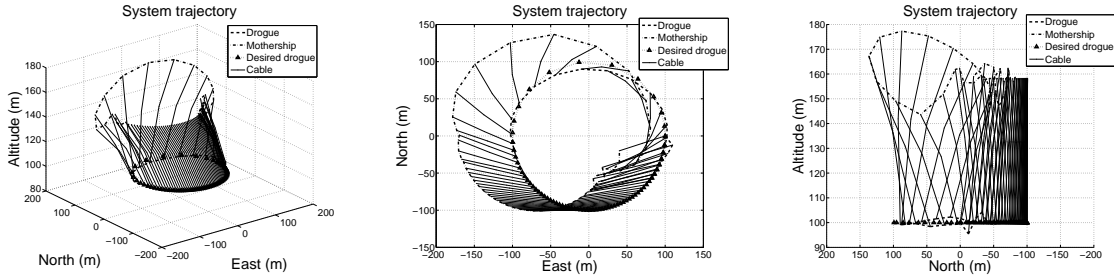


(a) Airspeed  $V_a$  vs. time.

(b) Flight path angle  $\gamma_a$  vs. time.

(c) Heading rate  $\dot{\psi}$  vs. time.

**Fig. 15** Evolution of constrained variables of the mothership using a desired drogue orbit with constant airspeed in the presence of 5 m/s wind from the west. All the constrained variables (solid lines) remained within their limits (dashed lines) except for the airspeed.



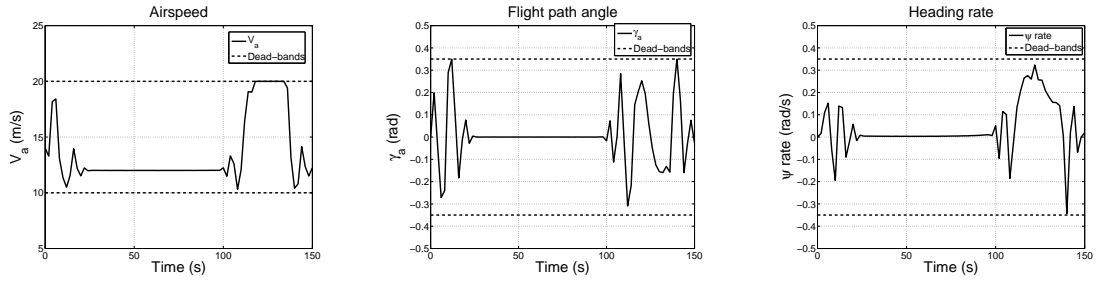
(a) 3-D view.

(b) Top-down view.

(c) Side view.

**Fig. 16** Optimal system trajectories using a desired drogue orbit with constant airspeed in the presence of 10 m/s wind from the west. The amplitude of the mothership's altitude oscillation was approximately 20 m. The waypoints placed close together when the system was flying upwind (towards the west), and sparse when the system was flying downwind (towards the east).

wind from the west. It can be seen that the offset of the mothership orbit center and the inclination of the desired mothership orbit become larger than those in Fig. 14. The actual drogue orbit shows both horizontal and vertical offsets, which imply the constrained variables of the mothership reached their limits during the flight. The mothership trajectory in Fig. 16 (c) may look unsmooth, but this is simply an effect of quantifying the trajectory waypoints. Figure 17 shows the evolutions of the constrained variables  $V_a$ ,  $\gamma_a$  and  $\dot{\psi}$  of the mothership. It can be seen that the desired airspeed of the mothership reached the limit, while  $\gamma_a$  and  $\dot{\psi}$  still remained within their limits.

(a) Airspeed  $V_a$  vs. time.(b) Flight path angle  $\gamma_a$  vs. time.(c) Heading rate  $\dot{\psi}$  vs. time.

**Fig. 17 Evolution of constrained variables of the mothership using a desired drogue orbit with constant airspeed in the presence of 10 m/s wind from the west. All the constrained variables (solid lines) were within their limits (dashed lines) except for the airspeed, which was at the upper limit for a fraction of the trajectory.**

### C. Transitions between Straight Level Flight and Orbital Flight

The transition between a straight and level flight and orbital flight (and vice versa) needs special attention for a towed cable system because the cable may become slack when the mothership turns and may experience large and sudden forces that may break the cable [7]. To prevent the tension forces exerted on the cable exceeding the loading limit of the cable, an optimal trajectory of the mothership is needed to keep the tension forces within their limits during the transition. In this section, we focus on the tow-in motion in which the system flies from a straight flight into an orbit. The tension forces on the cable are selected as additional constraints in the optimization with the limits  $\|\mathbf{T}_i\| \in [0, 10]$  N,  $i = 1, 2$ . Optimal results in different wind conditions are presented in this section.

Letting  $t_a$  be the time when transition started, the desired drogue trajectory in a tow-in motion can be written as

(1) when  $t \in [0, t_a]$ , the straight-line trajectory of the drogue is given by

$$p_{dr_n}^d(t) = -v_{dr}^g t$$

$$p_{dr_e}^d(t) = r_{dr}^d$$

$$p_{dr_d}^d(t) = -h_0;$$

(2) when  $t \in (t_a, t_1]$ , the circular trajectory of the drogue is given by

$$p_{dr_n}^d(t) = -v_{dr}^g t_a + r_{dr}^d \cos \theta(t)$$

$$p_{dr_e}^d(t) = r_{dr}^d \sin \theta(t)$$

$$p_{dr_a}^d(t) = -h_0.$$

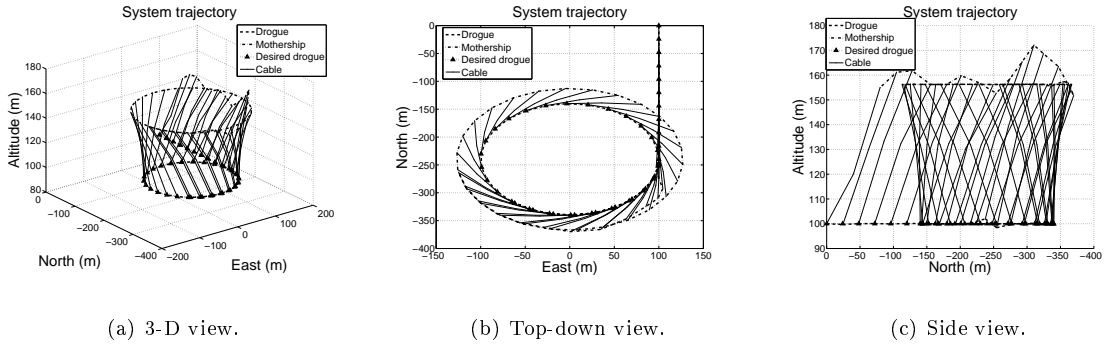
In this section, we use the desired circular drogue orbit with constant ground speed, i.e.,  $\theta(t) = v_{dr}^g t / r_{dr}^d$ . We select  $r_{dr} = 100$  m,  $v_{dr}^g = 12$  m/s,  $t_a = 20$  s and  $t_1 = 80$  s in the optimization algorithm. The initial configuration and solution results are shown in Table 4. When the wind increased to 10 m/s, the objective function value increased to 1751. This is because the existing performance limits of the mothership made the resulting optimal orbit unable to precisely place the drogue orbit onto the desired orbit.

**Table 4 Solution results of transitional flight in different wind conditions**

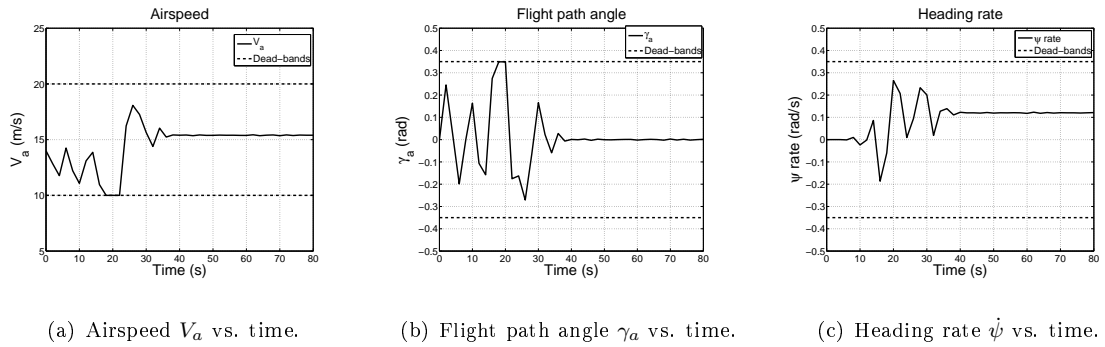
Wind speed (m/s)	$\mathbf{p}_m^0$ (m)	$\mathbf{v}_m^0$ (m/s)	Solution Time (s)	$\Phi$
0	(-80, 100, -155)	(-14, 0, 0)	23.2	20.3
$(0, 5, 0)^T$	(-80, 67, -155)	(-14, 0, 0)	20.1	21.6
$(0, 10, 0)^T$	(-70, 41, -143)	(-14, 0, 0)	29.7	1751.0
$\mathbf{p}_m^0$ = initial mothership position; $\mathbf{v}_m^0$ = initial mothership velocity in NED frame.				

Figure 18 shows the different views of the optimal system trajectories during a tow-in maneuver in the absence of wind. It can be seen that it takes one quarter circle for the mothership to complete the transition. The mothership trajectory had an altitude oscillation of approximately 20 m during the transition. Figure 19 shows the evolutions of the constrained variables  $V_a$ ,  $\gamma_a$  and  $\dot{\psi}$  of the mothership. It can be seen that the airspeed reached its lower limits during the transition. The large oscillation of  $\gamma_a$  explained the altitude oscillation of the mothership during the transition. Figure 20 shows the evolution of the tension forces on the cable in the transitional flight. The tension forces had a small oscillation (approximately 1 N), while remaining within their limits.

Figure 21 shows the different views of the optimal system trajectories during a tow-in maneuver in the presence of 5 m/s wind from the west. It can be seen that the mothership trajectory had an altitude oscillation of approximately 15 m during the transition. Figure 22 shows the evolutions



**Fig. 18** Optimal system trajectories in the transitional flight in the absence of wind. The mothership trajectory (dash-dot line) had an obvious altitude oscillation (approximately 20 m) during the transition and converged quickly to the desired orbit which place the drogue trajectory (dashed line) into the desired orbit (triangle-dot line).



**Fig. 19** Evolution of constrained variables of the mothership in the transitional flight in the absence of wind. The airspeed and flight path angle reached their limits during the transition.

of the constrained variables  $V_a$ ,  $\gamma_a$  and  $\dot{\psi}$  of the mothership. It can be seen that all the variables remained within the limits during the transition. Figure 23 shows the cable tension evolution during the transitional flight. It can be seen that the tension forces had an oscillation of approximately 2 N during the transition while they still remained within the limits.

Figure 24 shows the different views of the optimal system trajectories during a tow-in maneuver in the presence of 10 m/s wind from the west. It can be seen that the mothership trajectory had an altitude oscillation of approximately 10 m during the transition. Figure 25 shows the evolutions of the constrained variables  $V_a$ ,  $\gamma_a$  and  $\dot{\psi}$  of the mothership. It can be seen that  $V_a$  reached its upper bound while  $\gamma_a$  and  $\dot{\psi}$  remained within the limits during the transition. Therefore, the resulting optimal orbit unable to precisely place the drogue orbit onto the desired orbit, and this explains the

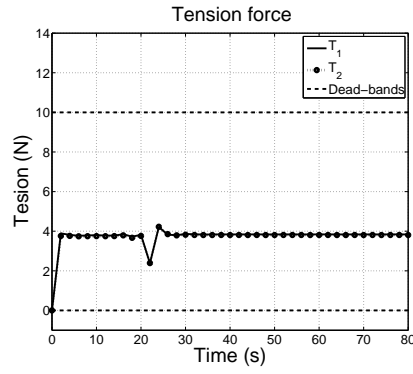


**Fig. 20** Evolution of the tension forces of the cable in the transitional flight in the absence of wind. The tension forces of the cable had a small oscillation during the transition, while they remained within their limits.

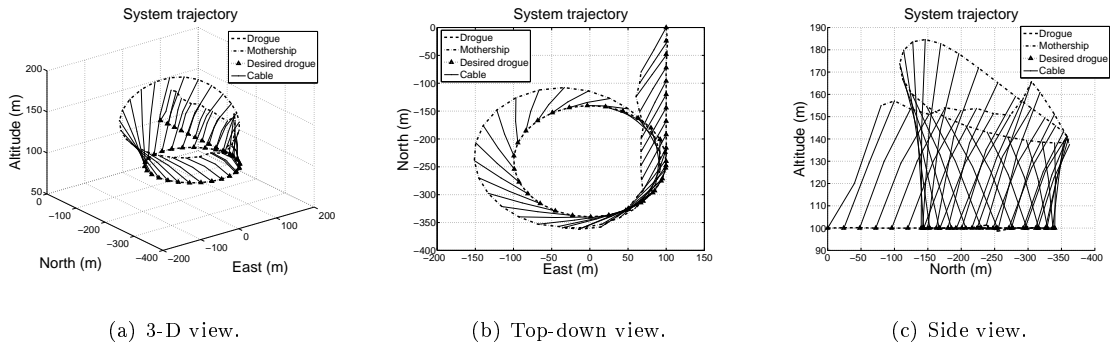
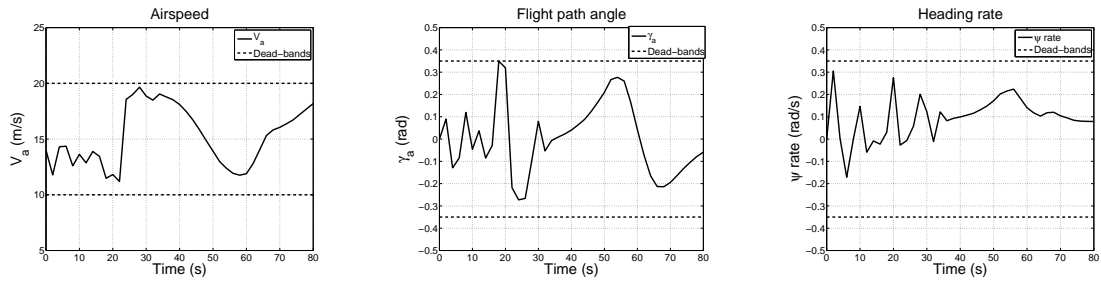


**Fig. 21** Optimal system trajectories in the transitional flight in the presence of 5 m/s wind from the west. The resulting optimal mothership orbit (dash-dot line) had a offset to the west of the drogue trajectory during the straight flight, experienced an altitude oscillation with amplitude of approximately 15 m during the transition, and converged to the desired orbit which place the drogue trajectory (dashed line) into the desired orbit (triangle-dot line).

large objective function value (1751) in Table 4. Figure 26 shows the cable tension evolution during the transitional flight. It can be seen that the tension forces had an increase (approximately 3 N), while they remained within the limits during the transition.

It can be seen that the altitude oscillation of the mothership increases as the wind speed increases. The tension forces only had small oscillations during the transition and remained within their limits.



(a) Airspeed  $V_a$  vs. time.

(b) Flight path angle  $\gamma_a$  vs. time.

(c) Heading rate  $\dot{\psi}$  vs. time.

**Fig. 22** Evolution of constrained variables of the mothership in the transitional flight in the presence of 5 m/s wind from the west. All the variables remained within their limits. The large oscillation of the flight path angle (15 s to 30 s) explains the oscillation of the mothership altitude during the transition.

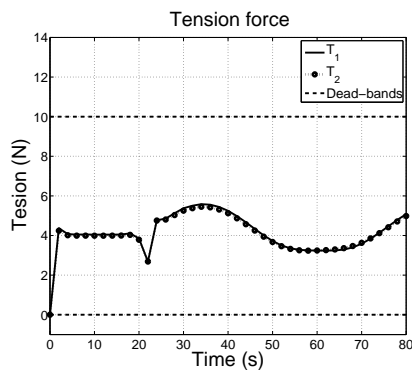


**Fig. 23** Evolution of the tension forces of the cable in the transitional flight in the presence of 5 m/s wind from the west. The tension forces of the cable had a small oscillation during the transition, while they remained within their limits.

## VI. Conclusion

This paper presents a strategy for generating optimal trajectories for the constrained towing vehicle (mothership) of an aerially towed cable system using MPC. To select an appropriate number of cable links in the optimization, model validation was conducted by comparing the flight test data with the results from the simulation with different numbers of cable link. The results indicate that a different number of cable links (1, 2, 5) did not result in a significant difference in the resulting motion. Two cable links were chosen as compromise between accuracy and complexity. The optimization formulation using model predictive control was presented by employing a combination of the squared-error and  $L_1$ -norm form objective function. Different desired drogue paths were

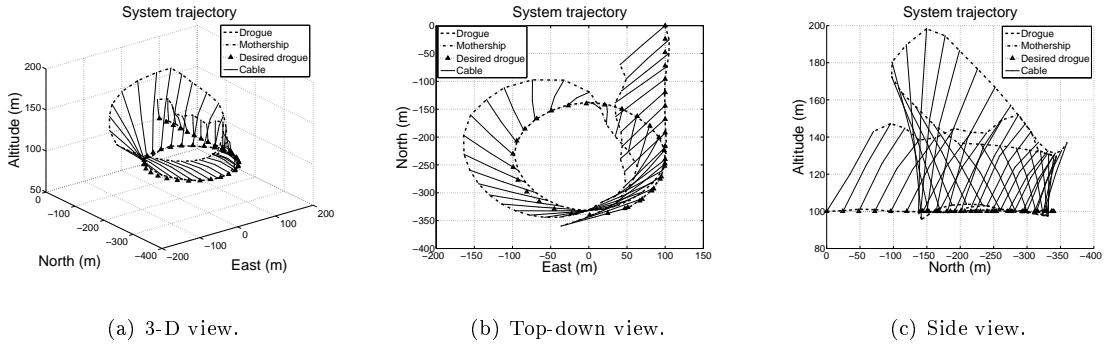


**Fig. 24** Optimal system trajectories in the transitional flight in the presence of 10 m/s wind from the west. The resulting optimal mothership orbit (dash-dot line) had a offset to the west of the drogue trajectory during the straight flight, experienced an altitude oscillation with amplitude of approximately 10 m during the transition, and converged to the desired orbit which place the drogue trajectory (dashed line) into the desired orbit (triangle-dot line).

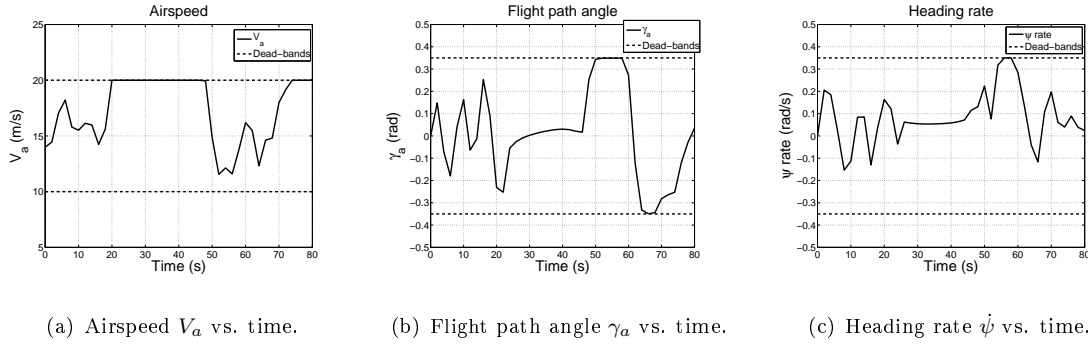


**Fig. 25** Evolution of constrained variables of the mothership in the transitional flight in the presence of 10 m/s wind from the west. The airspeed reached its limit during the transition, while the flight path angle and heading rate remained within their limits. The large oscillation of the flight path angle (15s to 30s) explains the oscillation of the mothership altitude during the transition.

employed to examine the strategy of the optimal trajectory generation. For the desired drogue orbits with constant ground speed, stronger wind required larger maneuvers on both the airspeed and flight path angle of the mothership, while for the desired drogue orbits with constant airspeed, stronger wind required larger maneuvers only on the airspeed of the mothership. In the transitional flight, as the wind increased, the altitude oscillation of the mothership during the transition decreased. The tension forces on the cable were also kept within the limits during the transition. This MPC-based optimal trajectory generation strategy can be a framework for specifying any arbitrary flight path

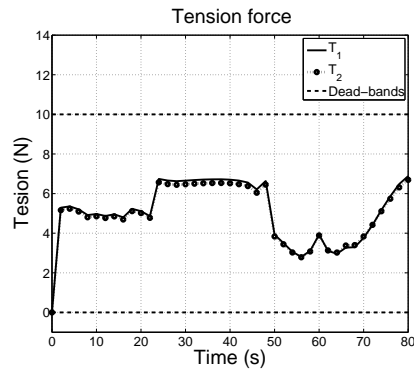


**Fig. 26 Evolution of the tension forces of the cable in the transitional flight in the presence of 10 m/s wind from the west. The tension forces of the cable had a major elevation during the transition, while they remained within their limits.**

of the towed body by optimizing the action of the towing vehicle subject to constraints and wind disturbance.

#### Acknowledgment

This research was supported by the Air Force Office of Scientific Research under STTR contract No. FA 9550- 09-C-0102 to Procerus Technologies and Brigham Young University.

#### References

- [1] Kolodner, I., "Heavy rotating string – a nonlinear eigenvalue problem," *Communications on Pure and Applied Mathematics*, Vol. 8, 1955, pp. 395–408.
- [2] Skop, R. A. and Choo, Y., "The Configuration of a Cable Towed in a Circular Path," *Journal of Aircraft*, Vol. 8, No. 11, November 1971, pp. 856–862.
- [3] Zhu, F. and Rahn, C. D., "Stability Analysis of a Circularly Towed Cable-body System," *Journal of Sound and Vibration*, Vol. 217, No. 3, May 1998, pp. 435–452.
- [4] Yamaguchi, S., Koterayama, W., and Yokobiki, T., "Development of a motion control method for a towed vehicle with a long cable," *Proceedings of the 2000 International Symposium on Underwater Technology*, Tokyo, Japan, May 2000, pp. 491 – 496.
- [5] Lambert, C. and Nahon, M., "Stability Analysis of a Tethered Aerostat," *Journal of Aircraft*, Vol. 40, No. 4, 2003, pp. 705–715.

- [6] Williams, P. and Trivailo, P., “Dynamics of Circularly Towed Cable Systems, Part 1: Optimal Configurations and Their Stability,” *AIAA Journal of Guidance, Control, and Dynamics*, Vol. 30, No. 3, May-June 2007, pp. 753–765.
- [7] Williams, P. and Trivailo, P., “Dynamics of Circularly Towed Cable Systems, Part 2: Transitional Flight and Deployment Control,” *AIAA Journal of Guidance, Control, and Dynamics*, Vol. 30, No. 3, May-June 2007, pp. 766–779.
- [8] Williams, P. and Ockels, W., “Dynamics of Towed Payload System Using Multiple Fixed-Wing Aircraft,” *AIAA Journal of Guidance, Control, and Dynamics*, Vol. 32, No. 6, November-December 2009, pp. 1766–1780.
- [9] Williams, P., “Optimization of Circularly Towed Cable System in Crosswind,” *AIAA Journal of Guidance, Control, and Dynamics*, Vol. 33, No. 4, July-August 2010, pp. 1251–1263.
- [10] Choo, Y. and Casarella, M. J., “A Survey of Analytical Methods for Dynamic Simulation of Cable-Body Systems,” *Journal of Hydronautics*, Vol. 7, No. 4, 1973, pp. 137–144.
- [11] Murray, R., “Trajectory Generation For a Towed Cable System Using Differential Flatness,” *13th Triennial World Congress of the International Federation of Automatic Control*, 1996, pp. 395–400.
- [12] Williams, P., Lansdorp, B., and Ockels, W., “Optimal Cross-Wind Towing and Power Generation with Tethered Kites,” *AIAA Journal of Guidance, Control, and Dynamics*, Vol. 31, No. 1, 2008, pp. 81–93.
- [13] Williams, P., “Periodic Optimal Control of a Towed Aerial-Cable System in Presence of Cross-Wind,” *AIAA Guidance, Navigation, and Control Conference*, Keystone, Colorado, August 2006.
- [14] Williams, P., Laphorne, P., and Trivailo, P., “Circularly-Towed Lumped Mass Cable Model Validation from Experimental Data,” *AIAA Modeling and Simulation Technologies Conference and Exhibit*, Keystone, Colorado, August 2006.
- [15] Cochran, J. E. J., Innocenti, M., No, T. S., and Thukral, A., “Dynamics and Control of Maneuverable Towed Flight Vehicles,” *AIAA Journal of Guidance, Control, and Dynamics*, Vol. 15, No. 5, 1992, pp. 1245–1252.
- [16] Borst, R. G., Greisz, G. F., and Quynn, A. G., “Fuzzy Logic Control Algorithm for Suppressing E-6A Long Trailing Wire Antenna Wind Shear Induced Oscillations,” *AIAA Guidance, Navigation, and Control Conference*, August 1993.
- [17] Hover, F. S., “Experiments in Dynamic Positioning of a Towed Pipe,” *OCEANS '93. Engineering in Harmony with Ocean*, Vol. 3, Victoria, BC, Canada, Oct 1993, pp. III484 – III490.
- [18] Clifton, J. M., Schmidt, L. V., and Stuart, T. D., “Dynamic Modeling of a Trailing Wire Towed by an Orbiting Aircraft,” *AIAA Journal of Guidance, Control, and Dynamics*, Vol. 18, No. 4, 1995, pp. 875–

- [19] Sun, L. and Beard, R. W., "Towed Body Altitude Stabilization and States Estimation in Aerial Recovery of Micro Air Vehicles," *AIAA Guidance, Navigation, and Control Conference*, Toronto, Ontario Canada, August 2010.
- [20] Williams, P., Sgarioto, D., and Trivai, P., "Motion Planning for an Aerial-Towed Cable System," *AIAA Guidance, Navigation, and Control Conference*, August 2005.
- [21] Sun, L., Beard, R. W., and Colton, M. B., "Motion planning and control for mothership-cable-drogue systems in Aerial Recovery of Micro Air Vehicles," *American Control Conference*, Baltimore, MD, USA, 2010, pp. 2101 – 2106.
- [22] Sun, L. and Beard, R. W., "Towed-body Trajectory Tracking in Aerial Recovery of Micro Air Vehicle in the presence of Wind," *American Control Conference*, San Francisco, CA, USA, 2011, pp. 3209–3214.
- [23] Colton, M., Sun, L., Carlson, D., and Beard, R., "Multi-vehicle dynamics and control for aerial recovery of Micro Air Vehicles," *Int. J. Vehicle Autonomous Systems*, Vol. 9, 2011, pp. 78–107.
- [24] Sgarioto, D. E., *Non-linear Dynamic Modelling and Optimal Control of Aerial Tethers for Remote Delivery and Capture of Payloads*, Ph.D. thesis, School of Aerospace Mechanical and Manufacturing Engineering, RMIT University, June 2006.
- [25] Williams, P., "Optimal terrain-following for towed-aerial-cable sensors," *Multibody Syst Dyn*, Vol. 16, 2006, pp. 351–374.
- [26] Williams, P., Sgarioto, D., and Trivailo, P., "Optimal Control of an Aircraft-Towed Flexible Cable System," *AIAA Journal of Guidance, Control, and Dynamics*, Vol. 29, No. 2, March–April 2006, pp. 401–410.
- [27] Fliess, M., Levine, J., Martin, P., and Rouchon, P., "Flatness and defect of non-linear systems: introductory theory and examples," *International Journal of Control*, Vol. 61, No. 6, 1995, pp. 1327–1361.
- [28] Williams, P., Sgarioto, D., and Trivailo, P. M., "Constrained path-planning for an aerial-towed cable system," *Aerospace Science and Technology*, Vol. 12, 2008, pp. 347–354.
- [29] Qin, S. and Badgwell, T., "A survey of industrial model predictive control technology," *Control Engineering Practice*, Vol. 11, 2003, pp. 733–764.
- [30] Qin, S. and Badgwell, T., "An overview of industrial model predictive control technology," *Proc. CPC V*, 1997, pp. 232–256.
- [31] Qin, S. and Badgwell, T., *Nonlinear Model Predictive Control*, chap. An overview of nonlinear model predictive control applications, Birkhäuser Verlag, Boston, MA, 2000, pp. 369–392.
- [32] Binder, T., Blank, L., Bock, H., Burlisch, R., Dahmen, W., Diehl, M., Kronseder, T., Marquardt, W.,

- Schlöder, J., and Stryk, O., *Online Optimization of Large Scale Systems*, chap. Introduction to model based optimization of chemical processes on moving horizons, Springer-Verlag Berlin Heidelberg, 2001, pp. 295–339.
- [33] Albuquerque, J. and Biegler, L., “Decomposition Algorithms for On-Line Estimation with Nonlinear DAE Models,” *Computers and Chemical Engineering*, Vol. 21, No. 3, 1997, pp. 283–299.
- [34] Diehl, M., Bock, H. G., Schlöder, J. P., Findeisen, R., Nagy, Z., , and Allgöwer, F., “Real-time optimization and nonlinear model predictive control of processes governed by differential-algebraic equations,” *Journal of Process Control*, Vol. 12, 2002, pp. 577–585.
- [35] Wächter, A. and Biegler, L., “On the Implementation of a Primal-Dual Interior Point Filter Line Search Algorithm for Large-Scale Nonlinear Programming,” *Mathematical Programming*, Vol. 106, No. 1, 2006, pp. 25–57.
- [36] Haseltine, E. and Rawlings, J., “Critical Evaluation of Extended Kalman Filtering and Moving-Horizon Estimation,” *Ind. Eng. Chem. Res.*, Vol. 44, No. 8, 2005, pp. 2451–2460.
- [37] Odelson, B., Rajamani, M., and Rawlings, J., “A new autocovariance least-squares method for estimating noise covariances,” *Automatica*, Vol. 42, No. 2, February 2006, pp. 303–308.
- [38] Hedengren, J. and Edgar, T., “Moving Horizon Estimation - The Explicit Solution,” *Proceedings of Chemical Process Control (CPC) VII Conference*, Lake Louise, Alberta, Canada, 2006.
- [39] Spivey, B., Hedengren, J., and Edgar, T., “Monitoring of Process Fouling Using First-Principles Modeling and Moving Horizon Estimation,” *Proc. Texas, Wisconsin, California Control Consortium (TWCCC)*, Austin, TX, 2009.
- [40] Hedengren, J., Allsford, K., and Ramlal, J., “Moving Horizon Estimation and Control for an Industrial Gas Phase Polymerization Reactor,” *Proceedings of the American Control Conference (ACC)*, New York, NY, 2007, pp. 1353–1358.
- [41] Darby, M., Nikolaou, M., Jones, J., and Nicholson, D., “RTO: An overview and assessment of current practice,” *Journal of Process Control*, Vol. 21, 2011, pp. 874–884.
- [42] Hedengren, J., “APMonitor Modeling Language,” [apmonitor.com](http://apmonitor.com), Dec 2011.
- [43] Sun, L., Beard, R. W., Colton, M. B., and McLain, T. W., “Dynamics and Control of Cable-Drogue System in Aerial Recovery of Micro Air Vehicles Based on Gauss’s Principle,” *American Control Conference*, St. Louis, MO, USA, June 2009, pp. 4729–4734.
- [44] Bourmistrov, A. S., Hill, R. D., and Riseborough, P., “Nonlinear Control Law for Aerial Towed Target,” *AIAA Journal of Guidance, Control, and Dynamics*, Vol. 18, No. 6, 1995, pp. 1232–1238.
- [45] Quisenberry, J. E. and Arena, A. S., “Dynamic Simulation of Low Altitude Aerial Tow Systems,” *AIAA*

*Atmospheric Flight Mechanics Conference and Exhibit*, Vol. 1, Providence, Rhode Island, August 2004, pp. 243–252.

[46] Wächter, A. and Biegler, L. T., “On the Implementation of a Primal-Dual Interior Point Filter Line Search Algorithm for Large-Scale Nonlinear Programming,” *Mathematical Programming*, Vol. 106, No. 1, 2006, pp. 25–57.

[47] <http://apmonitor.com/wiki/index.php/Main/SlackVariables>